Simulation-based Assessment of Marker Placement for Point Cloud Acquisition using a Lunar Survey Rover

Tomoki S. [1*], Rikako S. [1], Keitaro K. [2], Masanori T. [2], Taizo K. [3], Masafumi N. [1]

[1]Shibaura Institute of Technology, Japan

[2]Asia Air Survey Co., Ltd. Japan

[3]Ritsumeikan University, Japan

*ah20086@shibaura-it.ac.jp

Abstract: *Recently, the Ministry of Land, Infrastructure, Transport and Tourism has promoted a project to develop innovative unmanned technologies for construction activities on the Moon through the Space Unmanned Construction Innovation Technology Development Promotion Project. The purpose of this project is to promote the construction of the world's first lunar base and, to further develop and disseminate unmanned construction technologies. These technologies will be applied to projects on Earth to cope with increasingly severe disasters, enhance national land resilience, and address the decline in population. These goals have stimulated discussions on the technological development of lunar base construction. Unmanned surveying and remote construction technologies are essential for the initial ground surveying in lunar base construction projects. However, extreme temperature changes and space radiation in the lunar environment make it difficult to conduct conventional surveying using a total station. Conventional simultaneous localization and mapping using LiDAR (LiDAR-SLAM) is suitable for 3-D measurement in a non-GNSS environment. However, LiDAR-SLAM is not suitable for lunar surfaces due to the regolith's poor geometric features. Therefore, we proposed a methodology using spherical markers as landmarks with LiDAR-SLAM to improve the self-position estimation performance. However, the design of the marker placement has not yet been discussed. Therefore, we conducted an experiment on spherical marker arrangement for LiDAR-SLAM to evaluate its relative accuracy. In this study, we evaluated the validity of the marker placement and simulated a reduction in the number of markers using data acquired in a lunar surface simulation field and a robot simulator that reconstructed the experimental field. We acquired point clouds of the lunar surface simulation field using LiDAR mounted on the prototype rover. In addition, we selected Webots as a robot simulator. Through our experiments, we applied a multivariate analysis to quantitative variables, such as the relative distance and angle between the spherical markers and the LiDAR. We also, propose a methodology to evaluate marker placement planning.*

Keywords: *LiDAR-SLAM, robot simulator, unmanned surveying*

Introduction

The Ministry of Land, Infrastructure, Transport and Tourism (MLIT) has recently been promoting a project to develop innovative unmanned construction technologies for construction activities on the Moon. This project is called the Space Unmanned Construction Innovation Technology Development Promotion Project. The MLIT considers remote or automated construction technology, such as unmanned construction, to be an important element in the construction of the world's first lunar base for space exploration. The MLIT also states that Japan's unmanned construction technology, which has overcome

many disasters in the past, is a strength on the international stage. In addition, to strengthen disaster preparedness in the face of increasingly severe disasters and a declining working population, the project aims to further advance and disseminate unmanned construction technology at construction sites, develop technology adapted to lunar base construction, and extend the technology to lunar exploration projects. These efforts have stimulated the development of lunar base construction technology. Unmanned surveying and remote construction technologies are essential for surveying the ground at the initial stage of a lunar base construction project. However, the lunar environment is subject to extreme temperature changes, and cosmic radiation in the lunar environment makes it difficult to conduct conventional surveying with a total station (TS), as is done on Earth. In addition, the lunar surface is entirely covered by regolith, an achromatic microtopography that lacks image and shape features. Therefore, simultaneous localization and mapping using LiDAR (LiDAR-SLAM) and Visual-SLAM using cameras are not suitable. LiDAR-SLAM, which uses spherical markers as landmarks, is considered to be suitable for topographic measurements on the Moon, and research is underway. However, the optimization of the marker placement planning has yet to be studied, which is an issue. Therefore, we conducted an experiment on spherical marker arrangement for LiDAR-SLAM to evaluate its relative accuracy. In this study, we evaluated the validity of the marker placement and simulated the reduction in the number of markers using data acquired in a lunar surface simulation field and a robot simulator that reconstructed the experimental field. We acquired point clouds of the lunar surface simulation field using LiDAR mounted on the prototype rover. In addition, we selected Webots as a robot simulator. Through our experiments, we applied a multivariate analysis to quantitative variables, such as the relative distance and angle between the spherical markers and the LiDAR. We also proposed a methodology to evaluate marker placement planning.

Literature Review

Two papers are listed as existing research. The first is a paper on validating SLAM and self-positioning estimation methods for autonomous remote construction on the Moon (Hamamoto et al., 2023). The lunar environment has significantly different gravity and soil conditions from the Earth, making it difficult to apply conventional terrestrial construction techniques directly. Therefore, based on the lunar base construction scenario proposed by the Japan Aerospace Exploration Agency (JAXA) International Space Exploration Center, the technological verification of excavation work in an environment that simulate the lunar

surface was conducted. In particular, this study examines the effectiveness of the SLAM technology in an environment without Global Navigation Satellite System (GNSS) cooperative control among multiple automated construction machines, and integrated technology for remote control and automatic control. The lunar surface has few feature points, which can cause degeneracy problems with conventional LiDAR-SLAM. However, it has been confirmed that mapping and self-position estimation can be performed correctly while avoiding degeneration by installing a temporary enclosure. Visual-SLAM is effective in environments where LiDAR-SLAM has difficulty capturing feature points. Second, a study examined the acquisition of high-density point clouds using LiDAR-SLAM. Conventional LiDAR-SLAM is difficult to apply in environments with poor geometrical features, such as the lunar surface. By contrast, structure from motion (SfM) and multi-view stereo (MVS) are superior at generating high-resolution 3-D models. However, challenges include determining the scale factor and achieving real-time processing. We propose a data acquisition method that integrates these technologies and is suitable for the lunar environment. We used JAXA's lunar exploration field as a test site to collect LiDAR data camera images from the lunar rover. First, point clouds were generated from the high-resolution camera images using SfM/MVS. LiDAR and AHRS were then combined to correct the acquired point clouds and determine the scale factors of cameras using the given sizes and relative positions of the markers. Finally, the SfM/MVS point clouds were registered to the LiDAR point clouds using the spherical markers, as well as scale and color information. The experimental results confirm that the red sphere markings effectively enable high-accuracy point cloud acquisition in the environment for both LiDAR-SLAM and SfM/MVS. However, the optimization of the marker placement remains a challenge that has not yet been investigated.

Methodology

The proposed method in this study is shown in Figure 1. It is based on the premise that the input data are a time series of point clouds using a LiDAR mounted on a turntable. First, the time series LiDAR point clouds are combined using a rotation transformation that reflects the rotation resolution of the turntable to generate point clouds around the LiDAR. We estimate the offsets that occur when mounting the LiDAR on the turntable, namely, vertical axis error, L-shaped frame tilt, and horizontal rotation axis error, and apply corrections on a frame-by-frame basis. Next, we extract and delete the ground surface from point clouds, followed by point cloud clustering processing. For each extracted cluster, we

apply boxes of varying sizes and extract only spherical point clouds. Clusters that do not meet the box conditions are deleted at this time, and the process moves on to the next cluster. This continues, until the last cluster, repeating the box-based processing. After that, based on spherical model fitting, we estimate the center position of the marker from the point clouds on the marker surfaces. The top of the spherical marker is obtained in advance using TS, and the data obtained by subtracting the radius of the spherical marker from the height is used as the most accurate value for the center position. The, residuals in the estimation are evaluated to ensure they meet the required accuracy.

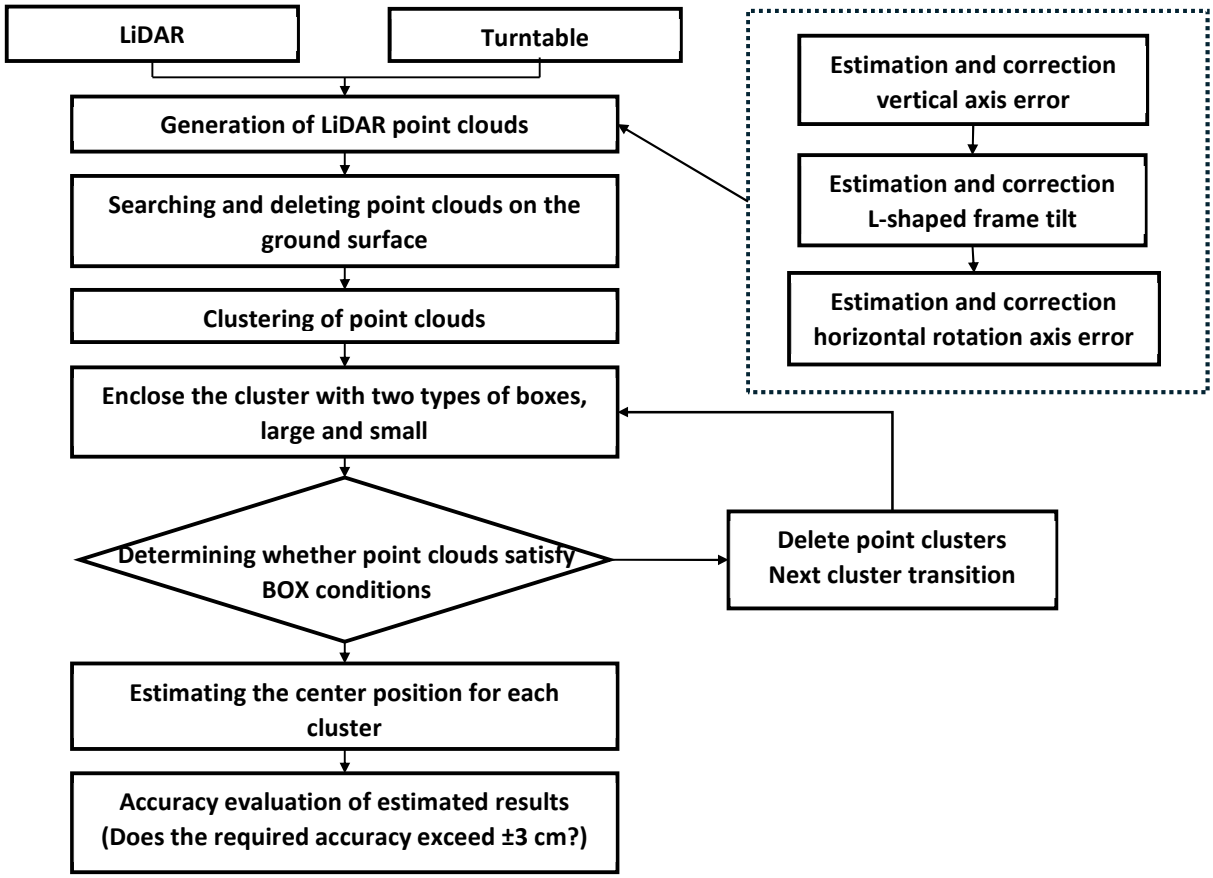

Figure 1: Evaluation Method for Placement Arrangement of Spherical Markers.

a. Turntable offset correction:

In this study, a turntable is installed on the top plate of a prototype rover and a LiDAR is attached to it. Point clouds are acquired by rotating the turntable. Three types of errors occur when attaching the LiDAR, namely, vertical axis error, L-shaped frame tilt, and horizontal rotation axis error, as shown in Figure 2. These errors decrease the accuracy of point cloud

synthesis, so correction processing is necessary to perform accurate landmark center position estimation.

First, the vertical axis error occurs when the LiDAR's optical axis is mounted slightly offset from the true vertical direction. This error is similar to the problem of direct and reverse observations in angular measurement. In this study, we apply a processing method modeled after the correction technique used in that field. Specifically, when measuring with a 360° LiDAR mounted vertically, the same area is measured from different frames. This occurs because when a frame is obtained and the turntable is rotated 180° horizontally, the resulting frame measures the same area from a different angle. Ideally, the two frames would match perfectly, however, if there is an error in the line-of-sight axis, even if the two frames are superimposed by rotation and translation, they will not match perfectly. This discrepancy is a manifestation of the vertical axis error. In this study, we use the iterative closest point (ICP) algorithm to minimize this error. When applying ICP, the reference frame is designated as positive, and the frame rotated 180° from the reference frame is designated as negative. By matching the two frames, the discrepancy between them is sequentially minimized, and the vertical axis error is estimated and corrected.

Next, we discuss the tilt of the L-shaped frame. This is an error that occurs when the L-shaped support frame to which the LiDAR is attached is tilted relative to the ideal vertical reference. If this tilt is not corrected when synthesizing point clouds, the point clouds of the entire environment will be superimposed at an angle from the horizontal, which makes it difficult to accurately estimate the center position of the marker. In this study, we apply the ICP algorithm again to estimate this error. Specifically, we compare the two frames used to estimate the vertical axis error, and correct it by optimizing the tilt of the L-shaped frame.

Horizontal rotation axis error occurs when there is a slight offset distance between the rotation axis of the turntable and the ideal vertical axis based on the center of the LiDAR. If this error is not corrected, unnatural variations occur in the point cloud obtained during rotation. It has been confirmed that this error becomes especially large, particularly when estimating the center position of spherical markers. In this study, spherical markers placed in the experimental field are used to estimate horizontal rotation axis error. Because the diameters of all the spherical markers are known, the markers can be used as a reference for spherical model fitting. Specifically, a spherical model with a known diameter is applied to the point clouds. Then, point cloud matching is performed using ICP to calculate the position where the point cloud distribution matched most closely. This allows us to estimate, the rotation axis offset.

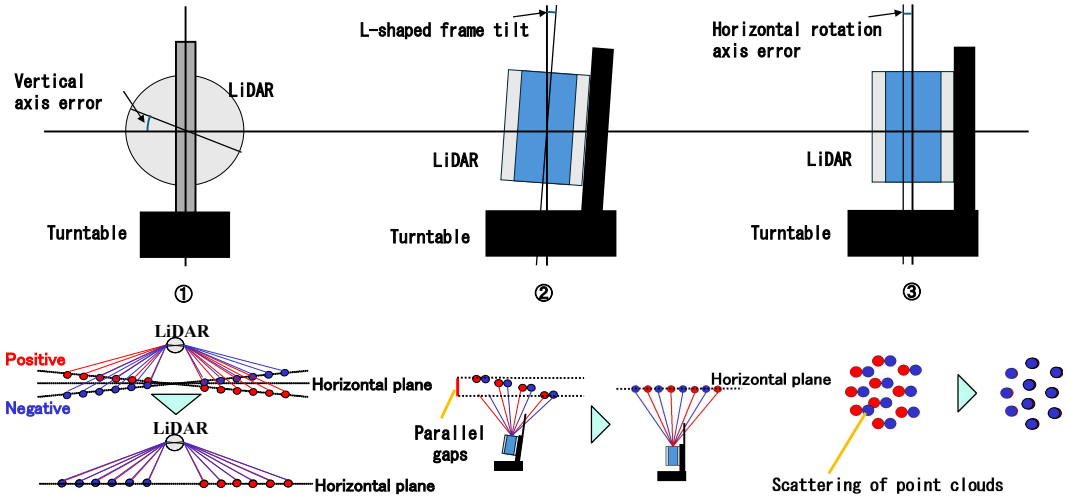

Figure 2: Horizontal Rotation 3-D-LiDAR Model Diagram.

b. Searching and extracting spherical point clouds:

The synthesized LiDAR point clouds include the spherical markers that are the measurement targets as well as point clouds of the ground surface vegetation, and other objects in the simulation field. Therefore, we first classify the point cloud using local elevation differences. Therefore, we classify the synthesized point clouds into grid data and extracted points within each grid where the z-coordinate increased by at least 0.2 m locally to find all point clouds of the spherical markers. Next, we classify the point clouds into clusters based on a specified Euclidean distance. For each cluster, we apply two types of cubes, large (with a side length of 0.30 m) and small (with a side length of 0.05 m), and determine which cube each cluster fits into, as shown in Figure 3. Specifically, if point clouds fit into the large cube but not the small cube, we judge that the cluster represents a marker. Furthermore, clusters containing a very small number of point clouds are likely to be noise, so they are removed from the clustering results. Figure 4 shows an example of the spherical point cloud extraction results.

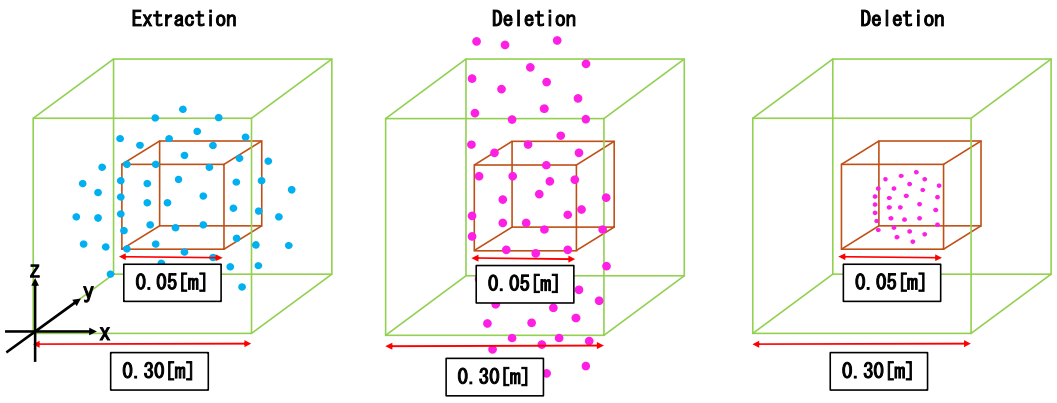

Figure 3: Extraction Process Using Two Types of Boxes.

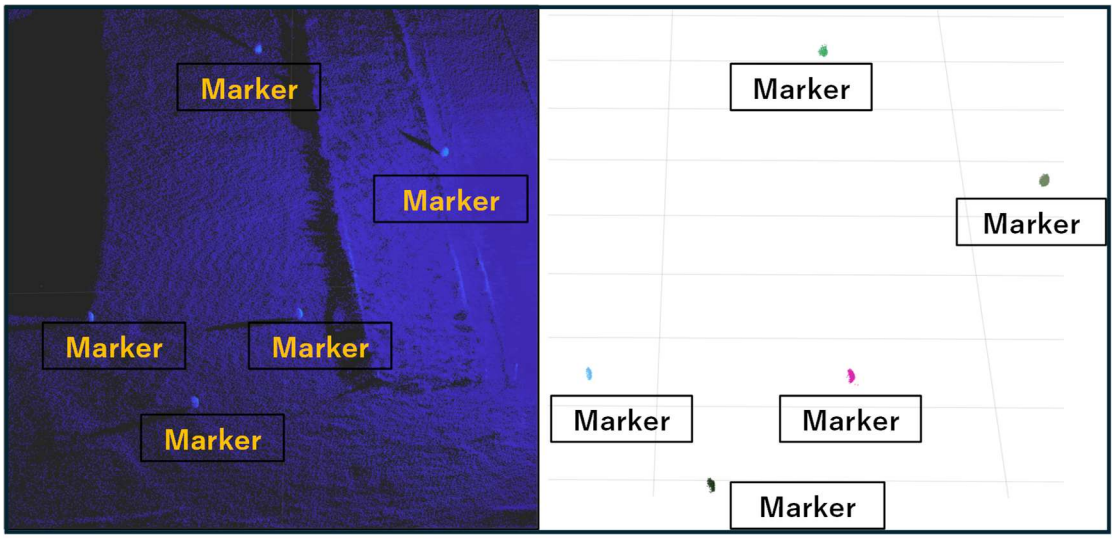

Figure 4: Point Clouds after the Box-based Processing.

c. Estimation of the center position of spherical markers:

Some of the marker point clouds may be deleted during the spherical point cloud search and extraction process due to the point cloud processing performed up to this point. Therefore, the spherical point cloud search is performed again. After extracting the spherical point cloud, the center of gravity of each cluster is calculated. For LiDAR point clouds that also include the ground surface, re-extracting point clouds within a 0.3 m radius centered on the calculated center of gravity selects, only the point clouds around the spherical marker. This makes subsequent processing easier. Using a hemispherical model with a known radius of the spherical marker as a reference, the center position of the marker is calculated by applying model fitting using ICP, as shown in Figure 5. ICP is a method that achieves alignment between two point clouds through repeated calculations by finding corresponding points and repeatedly transforming them to minimize the error. Therefore, using a 3-D spherical model as the reference model requires a complex algorithm to find corresponding points, making it difficult to improve accuracy due to different data formats. In this study, the reference model is in point cloud format, and ICP processing is applied using point-to-point calculations.

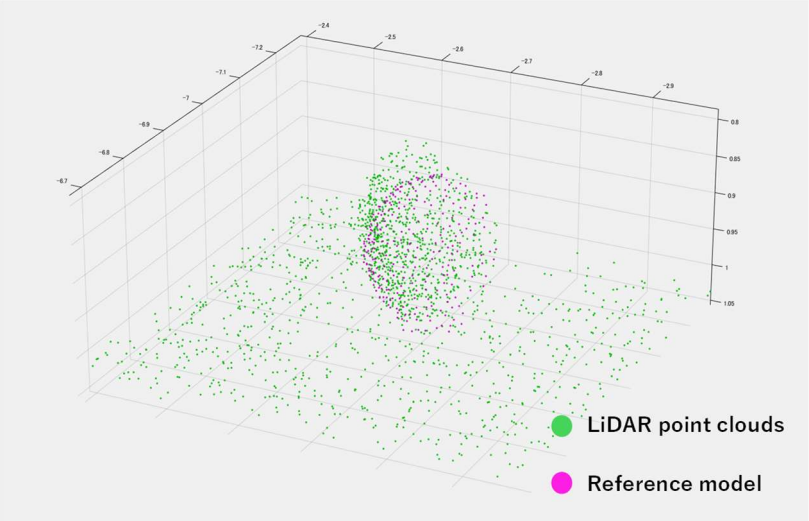

Figure 5: Model Fitting Process.

Experiment

We constructed an experimental field at Nippon Yakin Kogyo Co., Ltd. in Kyoto to simulate a lunar environment for conducting crater formation and soil and ground surveys, as shown in Figure 6. The experimental field contains 11 red and 0.20m diameter spherical markers, which were visible from three or more directions at each measurement position. Point clouds were acquired at seven positions using a rover-mounted LiDAR and cameras. The prototype rover was equipped with a 3-D-LiDAR (VLP-16, Velodyne) mounted on a turntable (PT-LAN50, Carina System) at a position approximately 1.0 m above the ground surface. The server, which was mounted on the rover, remotely operated these measurement devices and connected to a terminal computer using a Wi-Fi router (WXR-5700AX7P, BUFFALO) to perform remote data acquisition within a range of 100 m in the experimental field. The 3-D-LiDAR was tilted at 90° to enable vertical scanning, and acquire a panoramic scene with horizontal rotation using the turntable as well as a conventional terrestrial laser scanner. However, the conventional terrestrial laser scanners do not support a self-calibration function. Therefore, for this experiment, we developed a self-calibration methodology for the horizontal rotation 3-D-LiDAR. Moreover, we evaluated our methodology by verifying the accuracy of the registration results of LiDAR point clouds acquired from multiple locations. For the LiDAR point clouds' registration evaluation, we used the measurement results obtained using a TS as the true values. In addition, experiments were conducted using a simulator (Webots) to evaluate the appropriateness of the marker placement during the experiment. By reproducing the LiDAR, spherical markers, and turntable rotation resolution in the robot simulator, we constructed an environment in which LiDAR point clouds similar to actual data could be obtained, as shown

in Figure 7. Multiple spherical markers were placed within a range of 1.0 to 50.0 m, at 1.0 m intervals within the 1.0 to 15.0 m range, at 2.0 m intervals within the 15.0 to 25.0 m range, and at 5.0 m intervals within the 25.0 to 50.0 m range. We collected point clouds with 800 scan frames at each measurement point.

LiDAR(VLP-16, Velodyne)	
Distance measurement accuracy	3cm
Angle resolution(Horizaontal axis)	0.25 deg
Angle resolution(Vertical axis)	2 deg
Measurement range(Horizontal axis)	360 deg
Measurement range(Vertical axis)	±15 deg
Sampling rate	10 Hz

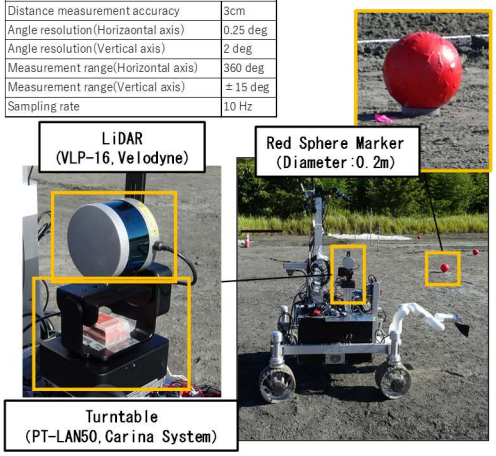

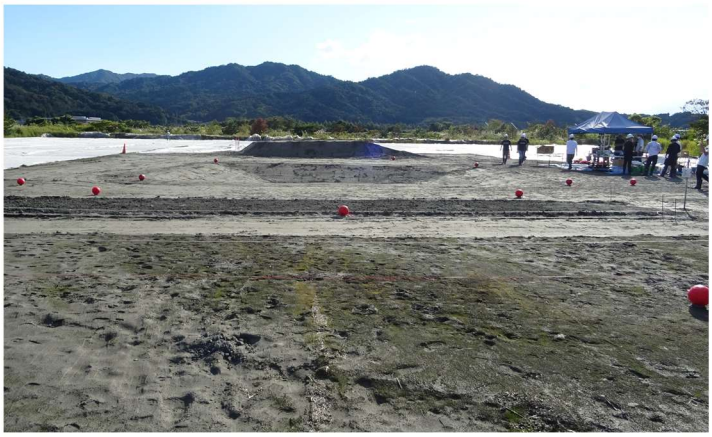

Turntable(PT-LAN50,)	
Mountable equipment weight	1.5kg
Pan rotation range	±170°
Tilt rotation range	±174°
Pan rotation speed	0.4° /s～50° /s
Tilt rotation Speed	0.4° /s～50° /s
External dimension	161.0(W)×161.5(H)×121.0(D)mm
Weight	2.26kg

Figure 6: Experimental Scene and Measurement Equipment.

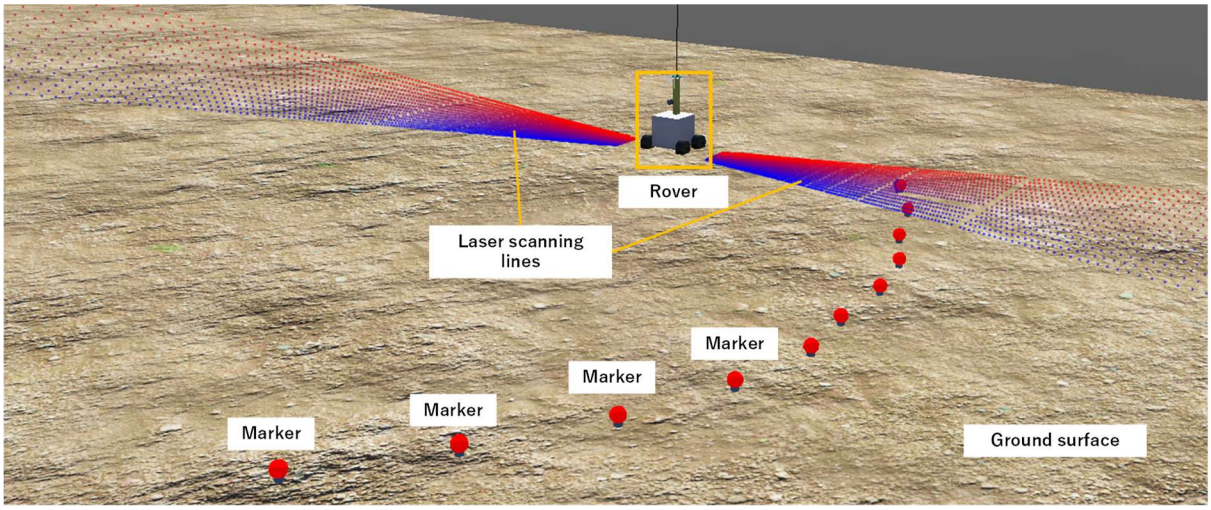

Figure 7: Robot Simulator Environment.

Results

Figure 8 shows the LiDAR point clouds synthesized with turntable offset correction. Table 1 shows the estimated center positions of the markers at each measurement position in experiments conducted on a robot simulator. Moreover, Table 2 summarizes the changes in point density that accompany changes in the distance between the LiDAR and the marker, evaluating the accuracy of the generated LiDAR point clouds based on the residuals during registration, using the measurement results from the TS as a reference. We compared the lengths of each edge by comprehensively connecting all spherical markers placed in the experimental field. Then we calculated the residuals based on the TS measurement results, and summarized the average estimated error for each measurement position in Figure 9.

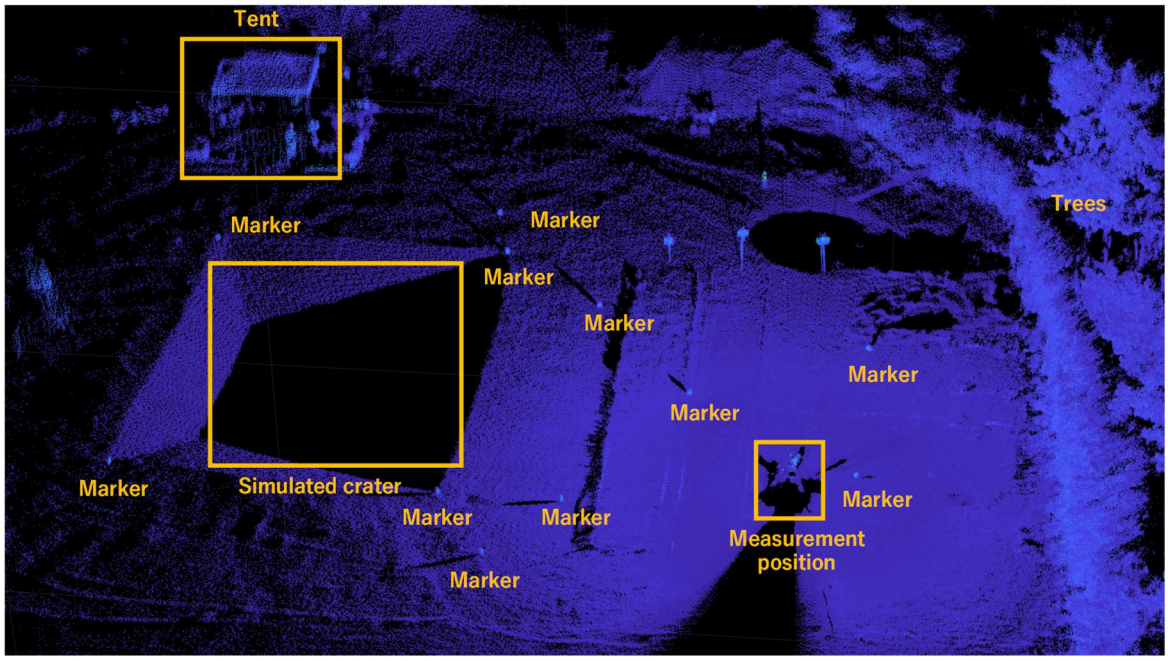

Figure 8: Rotating Synthetic Point Clouds.

Table 1: Point Density and Estimation Error by Distance.

Relative distance[m]	9.868	10.821	11.825	12.845	13.816	14.811	16.818	18.779	20.797	22.771	24.803	29.728	34.858	39.738	44.674	49.699
Point density[point/cm^3]	0.020	0.024	0.025	0.024	0.026	0.008	0.009	0.010	0.007	0.005	0.009	0.005	0.003	0.003	0.002	0.002
Estimation error[m]	0.010	0.009	0.007	0.009	0.006	0.008	0.008	0.011	0.019	0.016	0.009	0.009	0.022	0.017	0.074	0.075

Table 2: Relationship Between LiDAR-Marker Distance and Point Density.

			Marker ID										
			M1	M2	M3	M4	M5	M6	M7	M8	M9	M10	M11
Measurement position	1	Point density[point/cm^3]	0.058	0.023	0.086	0.024	0.007	0.006	0.004	0.016	0.095	0.044	0.008
		LiDAR-marker distance[m	8.227	10.237	7.347	11.194	21.862	28.088	24.887	16.870	6.129	12.189	19.302
	2	Point density[point/cm^3]	0.014	0.019	0.186	0.011	0.005	0.846	0.007	0.009	0.067	0.039	0.024
		LiDAR-marker distance[m	15.309	11.701	4.850	14.416	23.420	2.273	26.425	21.766	7.465	11.918	13.744
	3	Point density[point/cm^3]	0.010	0.018	0.019	0.010	0.016	0.166	0.060	0.098	0.181	0.024	0.012
		LiDAR-marker distance[m	18.491	16.229	15.229	14.674	21.184	5.580	9.441	7.585	5.661	15.403	16.015
	4	Point density[point/cm^3]	0.037	0.059	0.058	0.051	0.024	0.037	0.026	0.066	0.034	0.023	
		LiDAR-marker distance[m	10.987	9.016	8.504	9.706	12.249	11.244	11.106	8.344	9.222	11.822	
	5	Point density[point/cm^3]	0.016	0.030	0.130	0.231	0.166	0.012	0.036	0.015	0.015	0.014	0.016
		LiDAR-marker distance[m	16.447	11.605	5.442	4.809	5.687	19.454	10.254	15.948	18.455	20.277	16.887

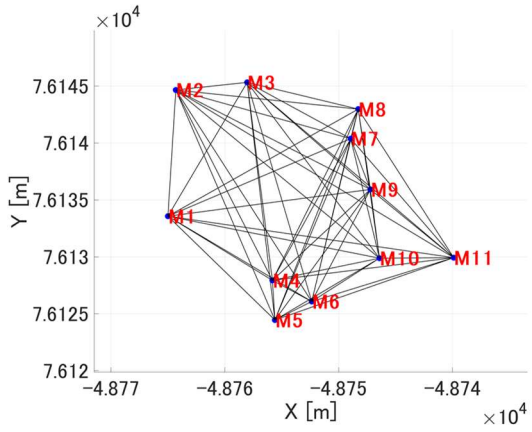

Measurement position	Estimation error (Average) [m]
1	0.011
2	0.010
3	0.011
4	0.012
5	0.009

Figure 9: Estimated Error at Each Measurement Position.

Discussion

Figure 10 shows the estimated center position based on experiments conducted with a robot simulator. We confirmed that under the rotational resolution of the turntable used in this study, an estimation accuracy of ±3 cm can be achieved, corresponding to the LiDAR ranging accuracy, when the distance between the LiDAR and the markers is within 40 m. This result indicates that the model fitting and point cloud synthesis functions operate with high accuracy under ideal environmental conditions within the simulator environment. However, ideal conditions do not exist in the actual lunar environment. The terrain often contains irregular features such as rocks, craters, and subtle undulations or slopes. When spherical markers are placed at 40-meter intervals, these conditions may cause occlusion effects, obscuring portions of the marker point clouds and resulting in incomplete or insufficient point cloud data acquisition. Therefore, rather than relying on simply placing markers at regular intervals, it is necessary to adopt a flexible placement plan that considers the terrain conditions. Furthermore, experimental results in the actual environment show

that the average error in estimating the center position of the markers at each measurement location is within ±3 cm. This indicates that performance equivalent to the ranging accuracy of LiDAR has been achieved. In addition, the marker placement conditions set in this study have been confirmed to sufficiently meet the ±10 cm construction requirement accuracy. However, as shown in Figure 11, some spherical point clouds were missing when extracting spherical markers from point clouds due to the influence of occlusion caused by simulated craters. In ICP-based model fitting, insufficient point density and missing point clouds can prevent residual minimization, which poses a risk of inaccurate. When using spherical markers as reference points, it is important to automatically exclude those with point cloud defects or incomplete formation, rather than using all markers in the field.

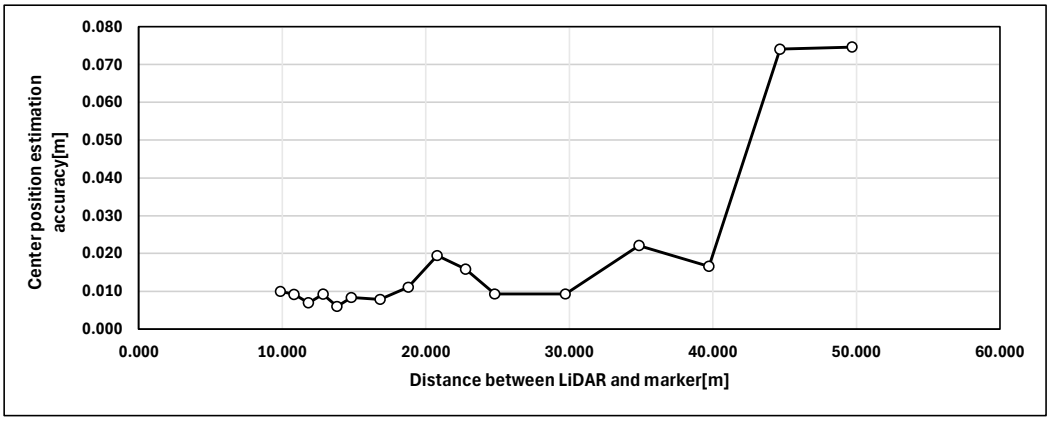

Figure 10: Relationship between Marker Distance and Center Position Estimation Accuracy.

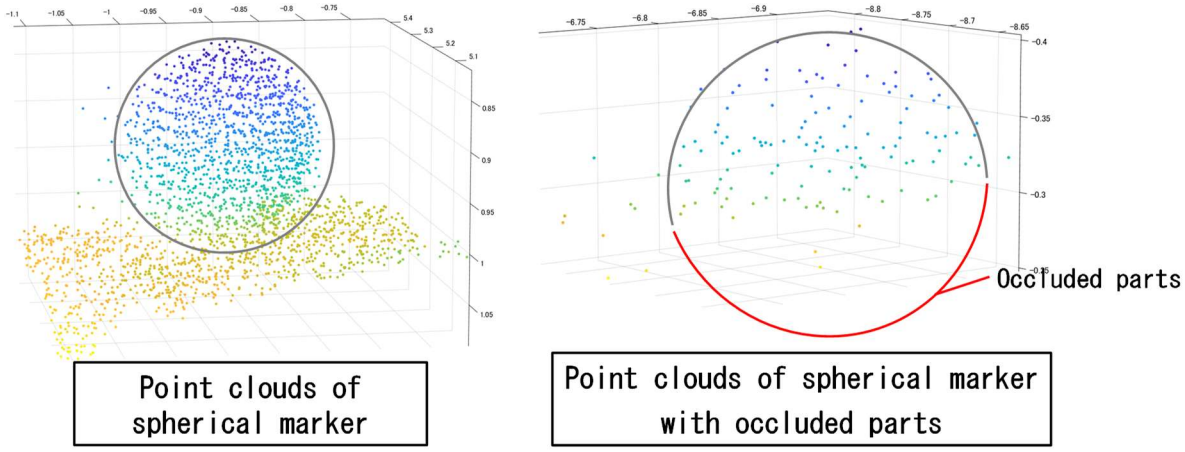

Figure 11: Comparison of Spherical Point Clouds.

Conclusion

In this study, we proposed a method for quantitatively evaluating the effectiveness of marker placement plans using point cloud data obtained from an experimental field equipped with

a lunar simulation environment and a robot simulator environment. Based on the results of experiments conducted in the robot simulator environment, we confirmed that when using the VLP-16, errors can be kept within the range of the LiDAR's ranging accuracy when the distance between the LiDAR and the markers was within approximately 40 m. Moreover, based on the experimental results conducted in the real environment, we confirmed that the ±10 cm construction requirement accuracy could be met under the marker placement conditions set in this experiment. However, simulations involving a reduction in the number of markers and the resulting changes in estimation accuracy have not been sufficiently evaluated. Therefore, an important future task is to quantify the trade-off between the number of markers and accuracy, as well as to establish evaluation metrics for achieving high-precision positioning with fewer markers.

Acknowledgements

This research was supported by the MLIT R&D Program for the Project of Technological Innovation for Construction on Space Field.

References

Hamamoto, K., Takagi, Y., Komatsu, S., Ishikawa, T., Miura, Sudo, M., Uchimura, Y., (2023). Development of autonomous remote construction technology adapted to the construction environment - space application of next generation construction systems. *Proceedings of the 67th Space Science and Technology Union.*

Shigefuji, R., Noguchi, K., Takigawa, M., Kitamura, K., Hiramatsu, T., Kobayashi, T., Nakagawa, M., (2023). Acquisition of Dense Point Clouds with LiDAR-SfM/MVS Lunar Environment. *Asian Conference on Remote Sensing (ACRS2023), p.6.*

Ministry of Land, Infrastructure, Transport and Tourism. Space Unmanned Construction Innovative Technology Development Promotion Project. 2023, from https://www.mlit.go.jp/report/press/kanbo08_hh_000959.html

Matthies, L., Daftry, S., Tepsuporn, S., Cheng, Y., Atha, D., Swan, R. M., Ravichandar, S., Ono, M., (2022). Lunar Rover Localization Using Craters as Landmark. *IEEE Aerospace Conference (AERO).*

Pedersen, L., Han, C. S., Vitus, M., (2008). Dark navigation: Sensing and rover navigation in permanently shadowed lunar craters. *In International Symposium on Artificial Intelligence, Robotics and Automation in Space (ISAIRAS).*

Pedersen, L., Allan, M., To, V., Utz, H., Wojcikiewicz, W., Chautems, C., (2010). High speed lunar navigation for crewed and remotely piloted vehicles. *ISAIRAS, Sapporo, Japan.*

Thrun, S., Montemerlo, M., Aron, A. (2006). Probabilistic Terrain Analysis for High-Speed Desert Driving. *Robotics Science and Systems Conference, Philadelphia.*

Campbell, S., O'Mahony, N., Carvalho, A., Krpalkova, L., Riordan, D., Walsh, J., (2020). Where am I? localization techniques for mobile robots a review. *6th International Conference on Mechatronics and Robotics Engineering (ICMRE), IEEE, pp. 43-47.*

Li, P., Wang, R., Wang, Y., Tao, W., (2020). Volume 8. Evaluation of the ICP Algorithm in 3D Point Cloud Registration. *IEEE, pp.68030-68048.*